Materials Science and Engineering B107 (2004) 204–216

www.elsevier.com/locate/mseb

Atomic-scale computations of the lattice contribution to thermal conductivity of single-walled carbon nanotubes

M. Grujicic [a,*], G. Cao [a], Bonnie Gersten [b]

[a] *Program in Materials Science and Engineering, Department of Mechanical Engineering, Clemson University, 241 Engineering Innovation Building, Clemson, SC 29634-0921, USA*

[b] *Army Research Laboratory—WMRD AMSRL-WM-MD, Aberdeen, Proving Ground, MD 21005-5069, USA*

Received 28 March 2002; accepted 17 November 2003

Abstract

The lattice contribution to thermal conductivity of single-walled carbon nanotubes with three different screw symmetry (chirality) is studied using the Green–Kubo relation from linear response theory and molecular dynamics based thermal current auto-correlation functions. The interactions between carbon atoms are analyzed using the Adaptive Intermolecular Reactive Empirical Bond Order (AIREBO) potential. The results obtained show that, due to an exponential-decay character of the long-time thermal current auto-correlation functions, quite accurate lattice thermal conductivities can be obtained using computational cells considerably smaller than the phonon mean free path. In addition, the computed lattice contributions to thermal conductivities are found to agree within a factor of two with their counterparts obtained using the Boltzmann transport equation. Also, chirality is found to affect lattice thermal conductivity by as much as 20%.

Keywords: Carbon nanotubes; Thermal conductivity; Fluctuation-dissipation theorem

1. Introduction

As the size of electronic and mechanical devices is reduced into nanometer length scale, materials thermal conductivity becomes an increasingly important since the operations of such devices may typically require that significant amounts of heat be dissipated in a small region. In general, however, experiment determination of thermal conductivity in nano-scale devices is quite difficult (e.g. [1]), particular in the case of devices with complex geometries. Fortunately, reliable theoretical and computational methods have been developed for predicting the thermal properties of nanoscale materials and devices (e.g. [2]).

Because of a remarkable combination of their properties (e.g. high hardness and stiffness, light weight, special electronic structure, high stability, etc.), carbon nanotubes are being considered as prime candidate materials for nano-scale device applications. Consequently, considerable effort has been invested in characterizing properties of carbon nanotubes, particularly their electronic and mechanical properties [3–6]. Surprisingly, despite the importance of thermal management in nano-scale devices, there has been relatively little progress in characterizing thermal conductivity of carbon nanotubes. This is partly due to challenges associated with nano-scale experimental measurements mentioned above, but it is also a result of technological difficulties of synthesizing high-quality, well-ordered nanotubes. Consequently, theoretical calculations of thermal conductivity of carbon nanotubes are presently very essential.

Theoretical calculations of thermal conductivity of materials can be classified as two main approaches: (a) first principles based atomistic simulations (e.g. [7–9]). This approach is particularly useful for nano-scale devices where the experimental determination of the thermal conductivity is quite challenging; and (b) continuum calculations based on transport theories such as the Boltzmann transport equation [10–12]. The main advantage of the continuum approach is that it enables an analysis of relatively large systems. However, the approach entails the knowledge of certain parameters such as phonon relaxation time and phonon density of states which must be determined using either experimental measurements (may be difficult in the

* Corresponding author. Tel.: +1-864-656-5639; fax: +1-864-656-4435.
E-mail address: mica.grujicic@ces.clemson.edu (M. Grujicic).

0921-5107/$ – see front matter © 2003 Elsevier B.V. All rights reserved.
doi:10.1016/j.mseb.2003.11.012

Report Documentation Page

Form Approved
OMB No. 0704-0188

1. REPORT DATE	2. REPORT TYPE	3. DATES COVERED
2004		**00-00-2004 to 00-00-2004**

4. TITLE AND SUBTITLE	5a. CONTRACT NUMBER
Atomic-scale computations of the lattice contribution to thermal conductivity of single-walled carbon nanotubes	5b. GRANT NUMBER
	5c. PROGRAM ELEMENT NUMBER
6. AUTHOR(S)	5d. PROJECT NUMBER
	5e. TASK NUMBER
	5f. WORK UNIT NUMBER
7. PERFORMING ORGANIZATION NAME(S) AND ADDRESS(ES) **Celmson University,Department of Mechanical Engineering,Clemson,SC,29634**	8. PERFORMING ORGANIZATION REPORT NUMBER
9. SPONSORING/MONITORING AGENCY NAME(S) AND ADDRESS(ES)	10. SPONSOR/MONITOR'S ACRONYM(S)
	11. SPONSOR/MONITOR'S REPORT NUMBER(S)

12. DISTRIBUTION/AVAILABILITY STATEMENT
Approved for public release; distribution unlimited

13. SUPPLEMENTARY NOTES

14. ABSTRACT

The lattice contribution to thermal conductivity of single-walled carbon nanotubes with three different screw symmetry (chirality) is studied using the Green?Kubo relation from linear response theory and molecular dynamics based thermal current auto-correlation functions. The interactions between carbon atoms are analyzed using the Adaptive Intermolecular Reactive Empirical Bond Order (AIREBO) potential. The results obtained show that, due to an exponential-decay character of the long-time thermal current auto-correlation functions, quite accurate lattice thermal conductivities can be obtained using computational cells considerably smaller than the phonon mean free path. In addition, the computed lattice contributions to thermal conductivities are found to agree within a factor of two with their counterparts obtained using the Boltzmann transport equation. Also, chirality is found to affect lattice thermal conductivity by as much as 20%.

15. SUBJECT TERMS

16. SECURITY CLASSIFICATION OF:			17. LIMITATION OF ABSTRACT	18. NUMBER OF PAGES	19a. NAME OF RESPONSIBLE PERSON
a. REPORT	b. ABSTRACT	c. THIS PAGE			
unclassified	**unclassified**	**unclassified**	**Same as Report (SAR)**	**13**	

case of nano-scale devices) or by theoretical calculations. An addition shortcoming of the continuum approach is that solving the governing integro-differential transport equation may be quite difficult in some cases.

Because of the aforementioned limitations of the continuum approach, the first principles based atomistic simulations are increasingly getting more attention as a means of predicting thermal properties. Besides not requiring the prior knowledge of the model parameters, atomic-scale calculations enable quantification of the effect of microstructure (e.g. phase interfaces and surface reconstruction) on thermal properties. Furthermore, atomistic simulations can be used to determine the parameters for the continuum models discussed above and, thus, help bridge gap between atomistic-scale and continuum-level calculations.

There are generally two main components of thermal conductivity of a material: (a) an electronic component which is controlled by the electronic band structure, electron scattering, and electron-phonon (lattice vibrations) interaction; and (b) a lattice component which is mainly controlled by phonons and phonon scattering. In the present paper, only the lattice contribution to thermal conductivity of carbon nanotubes is considered using atomistic simulations. It should be noted that the electronic contribution to thermal conductivity is very small and can be neglected only in materials with large band gaps. As far as carbon nanotubes are concerned, the size of their band gap is found to be dependent on their screw symmetry (chirality), as well as on their diameter and length. The largest band gap (on the order of 1.5 eV) is found in small diameter, short (n, m) nanotubes with the rollup vectors n and m satisfying the condition: $|n-m| \neq 3p$, where p is an integer. For other types of nanotubes, the band gap is considerably smaller approaching zero in the case of "arm chair" nanotubes in which $n = m$. For comparison, the band gap in a typical insulator is on the order of 5–10 eV and of a semiconductor in a range between 0.5 and 2.5 eV. Based on these observations, one may conclude that electronic contribution to the thermal conductivity can be significant in carbon nanotubes, particularly in those with metallic behavior, i.e. with a small band gap.

When thermal conductivity of solid crystalline materials is being calculated using atomistic simulations, due to a relatively large phonon mean-free path in such materials, one might expect that the size of the simulation cell on the order of several hundred nanometers must be used to prevent phonon scattering from the cell boundaries. In addition, quantification of phonon-phonon interactions (responsible for the finite values of thermal conductivity) is generally very complicated (e.g. [13]). In a recent study, Che et al. [2] carried out molecular dynamics simulations and used the linear-response theory based Green–Kubo equation and energy–current auto-correlation functions to determine thermal conductivity of diamond. They found that while the accuracy of the thermal conductivity is indeed dependent on the size of the periodic cell, an accurate thermal conductivity can be obtained using periodic cells about 40–60 times smaller than the actual phonon mean free path. They attribute this finding to the fact that the energy–current auto-correlation time is much shorter than the energy relaxation time. The approach of Che et al. [2] is used in the present work to determine the lattice contribution to thermal conductivity of single-walled carbon nanotubes of different chiralities.

The organization of the paper is as follows: a brief overview of the theoretical background related to the computation of thermal conductivity is given in Section 2.1. Section 2.2 and Appendix A contain details concerning the atomistic simulation procedure and the interatomic potential used. The main results obtained in the present work are presented and discussed in Section 3. The key conclusions resulting from the present work are given in Section 4.

2. Procedure

2.1. Theoretical background

At the macroscopic level, thermal conductivity is defined from the Fourier's law for steady-state heat conduction as:

$$\vec{J}_{\mathrm{q}} = -\Lambda \cdot \nabla T \tag{1}$$

where $\vec{J}_{\mathrm{q}}$ is the steady-state heat flux (current), Λ the thermal conductivity second-order tensor and ∇T the temperature gradient.

In general, the total energy current, $\vec{J}_{\mathrm{E}}$, includes the conduction heat current, $\vec{J}_{\mathrm{q}}$, and the diffusion energy current, $\mu\vec{J}$, where $\vec{J}$ is the particle current, and μ is the chemical potential. Thus, the following relation between the energy current and the heat current can be defined [14]:

$$\vec{J}_{\mathrm{q}} = \vec{J}_{\mathrm{E}} - \mu\vec{J}. \tag{2}$$

In solids under non-extremely high temperatures, the diffusion contribution to the energy current can be neglected.

In a system consisting of discrete particles, the energy density, $h(r)$, can be expressed (in the classical limit) as the site energy of each particle and consequently, the heat current can be defined as:

$$\vec{J}_{\mathrm{q}} = \frac{\mathrm{d}}{\mathrm{d}t}\sum_i \vec{r}_i h_i \tag{3}$$

where the raised arrow denotes a vector quantity, $\vec{r}$ the position vector, t is time and subscript i denotes particle i.

One approach to the determination of thermal conductivity by atomistic simulations is to place the computational cell in contact with two different reservoirs with temperatures T_1 and T_2 and to calculate the heat current when the system reaches the steady state. However, due to small dimensions of the computational cell (typically 10–50 nm edge side), even a small temperature difference of 10 K across the system gives rise to a thermal gradient on the order of 10^8 K/m. It is unlikely that the linear response theory (i.e. the linearity between the heat flux and the temperature gradient as

defined in Eq. (1)) would hold under such extreme thermal loading. Moreover, this temperature gradient maybe smaller than the thermal fluctuations in the system, making it difficult to obtain convergence of the simulation results within reasonable simulation times.

Due to the shortcomings of the approach discussed above, the fluctuation–dissipation theorem from the linear response theory which provides a connection between the energy dissipation in irreversible processes (heat conduction in the present case) and thermal fluctuations (of the heat current in the present case) of a system in equilibrium [15] is used in this work. Within this approach, the thermal conductivity tensor can be expressed in terms of heat-current auto-correlation functions, $C_J^C(t)$, [15,16] as:

$$\Lambda^{\mathrm{c}} = \frac{1}{k_{\mathrm{B}} T^2 V} \int_0^\infty \mathrm{d}t \, C_J^C(t) \tag{4}$$

where k_{B} is the Boltzmann's constant, T temperature, V volume and

$$C_J^C(t) = \langle \vec{J}_{\mathrm{q}}(t) \vec{J}_{\mathrm{q}}(0) \rangle. \tag{5}$$

$C_J^C(t)$ is obtained by phase (particles positions and momenta) space (Γ) averaging as:

$$\langle \vec{J}_{\mathrm{q}}(t) \vec{J}_{\mathrm{q}}(0) \rangle = \frac{\int \mathrm{d}\Gamma \exp(-\beta H) \vec{J}_{\mathrm{q}}(t) \vec{J}_{\mathrm{q}}(0)}{\int \mathrm{d}\Gamma \exp(-\beta H)} \tag{6}$$

where

$$H = \sum_i h_i. \tag{7}$$

within the framework of molecular dynamics simulations, Eq. (7) is evaluated as:

$$\langle \vec{J}(t) \vec{J}(0) \rangle = \frac{1}{N_{\mathrm{corr}}} \sum_{N_{\mathrm{corr}}} \vec{J}(t_0 + t) \vec{J}(t_0) \tag{8}$$

where

$$t = N_{\mathrm{t}} \, \Delta t, \quad 0 \le N_{\mathrm{t}} \le N_{\mathrm{MD}} \tag{9}$$

$$t_0 = N_0 \, \Delta t, \quad 0 \le N_0 \le N_{\mathrm{MD}} - N_{\mathrm{t}} \tag{10}$$

and

$$N_{\mathrm{corr}} = \mathrm{int}\left(\frac{N_{\mathrm{MD}}}{N_{\mathrm{t}}} \right), \tag{11}$$

where t and t_0 are, respectively, the current and the initial correlation times, Δt is the simulation time step, N_{MD} is the total number simulation steps, N_0 and N_{t} are integers, and int denotes operator for conversion of a real number to the closest smaller integer.

It should be noted that the analysis presented above is classical, i.e. no quantum effects are considered. In general, quantum effects are not critical when the temperature is significantly higher than the Debye temperature. While no information is available regarding the Debye temperature of carbon nanotubes, this temperature is expected to be considerably higher than the room temperature considering magnitudes of the Debye temperature in other forms of carbon. Using a quantum-physics based analysis, Che et al. [2] showed that in (hypothetical) purely-harmonic systems in which different phonon modes do not interact, quantum effects are negligible. In real systems, on the other hand, phonons are coupled and this anharmonicity is, in fact, responsible for a finite phonon mean free path, and hence, for finite thermal conductivity. Fortunately, thermal conductivity in such systems is dominated by low-frequency phonon modes, which are nearly classical. Hence, a lack of inclusion of the quantum corrections is generally considered not critical when calculating thermal conductivity. As far the anharmonicity effects are concerned, they are generally accounted for when (classical) molecular dynamics simulations based on realistic interatomic potentials are carried out and, hence, such simulations can be used, as is done in the present work, to determine thermal conductivity quite accurately.

2.2. Simulation procedure

Molecular dynamics simulations are conducted using computational cells which are of a finite size in one and infinitely long in the other two directions. The periodic boundary conditions are applied in the finite direction. Each cell contains a single (n, m) nanotube with the nanotube axis aligned with the direction in which the cell is finite. The dimension of the cell in the nanotube direction is varied in order to accommodate nanotubes of different chirality and, also, to explore the effect of the cell size on thermal conductivity. Three types of carbon nanotubes are studied in present work: (a) a (10, 10) armchair type nanotube; (b) a (18, 0) zig-zag type nanotube; and (c) a (14, 6) nanotube. The first nanotube is selected because it is frequently found in synthesized nanotube bundles, while the other two are selected on the basis that they have the diameter compatible to that of the (10, 10) nanotube. Other structural characteristics of the three nanotubes are given in Table 1 while the corresponding atomic arrangements are shown in Fig. 1(a)–(c).

The interactions between carbon atoms have been modeled using the Adaptive Intermolecular Reactive Empirical Bond-Order (AIREBO) potential developed by Stuart et al. [17]. This potential is an extension of the original Brenner's Reactive Empirical Bond-Order (REBO) potential [18] and includes non-bonding (intermolecular) atomic interactions.

Table 1
Structural characteristics of the carbon nanotubes studied in the preset work

Nanotube type (n, m)	Nanotube radius (nm)	Unit cell length (nm)	Number of atoms per unit cell
(10, 10)	1.351	0.2477	40
(18, 0)	1.404	0.4290	72
(14, 6)	1.387	3.8130	632

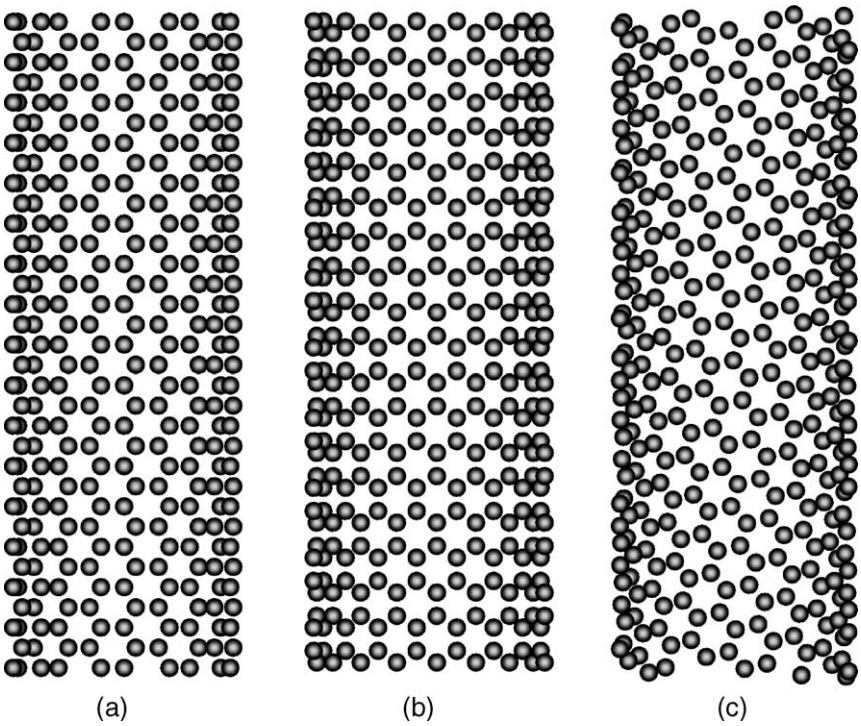

Fig. 1. Atomic configuration associated with: (a) a (10, 10) arm-chair nanotube; (b) a (18, 0) zig-zag nanotube; and (c) a (14, 6) nanotube of a general chirality.

It should be noted that while frequently the interactions between carbon atoms within a single single-walled carbon nanotubes are modeled using only the bonding part of an inter-atomic potential, the AIREBO potential used in the present work has been optimized to also include the non-bonding interactions between carbon atoms of the same single-walled carbon nanotube. Based on the AIREBO potential (reviewed briefly in Appendix A), the total potential energy be formally written as a summation of pair-wise interactions as [18]:

$$V_{\text{tot}} = \sum_i \sum_{j>i} V_{ij}. \tag{12}$$

Consequently, the energy of site i, h_i, can be defined as:

$$h_i = \frac{p_i^2}{2m_i} + \frac{1}{2}\sum_j V_{ij}. \tag{13}$$

However, since V_{ij} is, in fact, a many-body potential, the equation for heat current $J_{\text{q}}(t)$ based on Eq. (3) is somewhat complicated and, under the condition of a zero net momentum for the system, is given by:

$$\vec{J}_{\text{q}}(t) = \sum_i \vec{v}_i h_i + \tfrac{1}{2}\sum_{i,j}\sum_{k,l} \vec{r}_{ij}\vec{F}_{ij}^{kl} \cdot \vec{v}_i, \tag{14}$$

where

$$\vec{F}_{ij}^{kl} = -\frac{\partial V_{kl}}{\partial \vec{r}_{ij}}. \tag{15}$$

where $\vec{v}_i$ and ${}_i\vec{r}_{ij}$ are, respectively, the i-site velocity and the i–j sites relative position vector.

All molecular dynamics simulations are carried out in the present work using a fixed 1 fs time increment. For each simulation run, the system is equilibrated under isothermal ($T = 300$ K) conditions using Berendsen thermostat [19] for 40 ps. Subsequently, constant energy molecular dynamics simulations are carried out for 400 ps and the results used to calculating the heat current for every time step.

3. Results and discussion

3.1. The effect of computational cell size

As discussed earlier, the relative magnitudes of the computational cell size with respect to the phonon mean free path can be an important factor affecting the accuracy of thermal conductivity computed using atomistic simulations. When the simulation cell is too small, the time for phonons to travel through the simulation cell is shorter than the decay time of the heat-current auto-correlation function. This causes phonon scattering to take place more frequently than they would in an infinite system. In such cases, only the short time correlation functions are expected to be accurate. Nevertheless, Che et al. [2] showed that thermal conductivity can be computed using computational cells smaller than the phonon mean free path. Using the macroscopic laws of relaxation and the Onsager's postulate for microscopic thermal

Table 2
Optical and acoustic weighting factors, A_o and A_a, and relaxation times, τ_o and τ_a, obtained by nonlinear least squares fitting of the heat current autocorrelation function for (10, 10) armchair single-walled carbon nanotubes

Numbers of atoms	Cell length (nm)	A_o ($\times 10^{-6}$ J^2/cm^2)	τ_o (ps)	A_a ($\times 10^{-6}$ J^2/cm^2)	τ_a (ps)	$A_o\tau_o/A_o\tau_o + A_a\tau_a$
400	2.477	3.339	0.074	1.211	17.597	0.0012
800	4.954	3.334	0.070	1.216	17.870	0.0011
1600	9.908	3.299	0.072	1.227	17.940	0.0011
3200	19.816	3.376	0.069	1.232	17.851	0.0011
6400	39.632	3.339	0.070	1.230	17.877	0.0011
Average		3.343	0.070	1.229	17.869	

fluctuations, Che et al. [2] first showed that the long-time asymptotic decay of the heat-current auto-correlation function (which primarily controls thermal conductivity) is of an exponential type. Consequently, relatively short time simulation data obtained using medium-size computational cells can be used to determine quite accurately the exponential decay parameters of the heat-current autocorrelation function.

To determine the effect of the computational cell size on lattice thermal conductivity, five different sizes of the computational cell are used for each of the three carbon nanotubes analyzed in the present work. The number of atoms in the computational cell in each case is given in Tables 2–4. Due to the fact that the carbon nanotubes are single walled (one atomic layer thick), only thermal conductivity in the direction of nanotubes axis is computed. This is achieved by using only the data for thermal-energy current in the direction of nanotubes axis when calculating the auto-correlation functions, Eq. (5).

Examples of typical heat-current auto-correlation functions for the (10, 10), (18, 0) and (14, 6) nanotubes are shown in Fig. 2(a)–(c), respectively. These function are obtained using computational cells containing 3200, 2880 and 2528 atoms, respectively. In general, the auto-correlation functions are characterized by a rapid initial decay followed by a gradual, long-time exponential decay. The initial fast decay can be attributed to high-frequency optical phonon modes which are associated with out-of-phase vibrations of the atoms residing on two sub-lattices in the nanotube crystal structure. These phonons are scarcely populated and weakly coupled with low-frequency acoustic (in-phase vibrational) modes at room temperature and, hence, they do not significantly contribute to thermal conductivity. The long-time behavior of the heat-current auto-correlation functions and, hence, thermal conductivity are controlled by low-frequency acoustic phonon modes.

The auto-correlation function results such as the one shown in Fig. 2(a)–(c) are fitted using the Levenberg–Marquardt nonlinear least-squares method [23] to the following double exponential function:

$$C_J^C(t) = A_o \exp\left(\frac{-t}{\tau_o}\right) + A_a \exp\left(\frac{-t}{\tau_a}\right), \quad t \geq 0, \qquad (16)$$

where the subscript o and a are used to denote the optical and acoustic phonon modes, respectively. Substitution

Table 3
Optical and acoustic weighting factors, A_o and A_a, and relaxation times, τ_o and τ_a, obtained by nonlinear least squares fitting of the heat current autocorrelation function for (18, 0) zig-zag single-walled carbon nanotubes

Numbers of atoms	Cell length (nm)	A_o ($\times 10^{-6}$ J^2/cm^2)	τ_o (ps)	A_a ($\times 10^{-6}$ J^2/cm^2)	τ_a (ps)	$A_o\tau_o/A_o\tau_o + A_a\tau_a$
360	2.145	3.327	0.075	1.135	17.230	0.0013
720	4.290	3.329	0.071	1.141	17.306	0.0012
1440	8.580	3.338	0.073	1.150	17.395	0.0012
2880	17.160	3.330	0.071	1.153	17.349	0.0012
5760	34.320	3.344	0.069	1.150	17.401	0.0012
Average		3.338	0.070	1.150	17.375	

Table 4
Optical and acoustic weighting factors, A_o and A_a, and relaxation times, τ_o and τ_a, obtained by nonlinear least squares fitting of the heat current autocorrelation function for (14, 6) single-walled carbon nanotubes

Numbers of atoms	Cell length (nm)	A_o ($\times 10^{-6}$ J^2/cm^2)	τ_o (ps)	A_a ($\times 10^{-6}$ J^2/cm^2)	τ_a (ps)	$A_o\tau_o/A_o\tau_o + A_a\tau_a$
632	3.813	3.280	0.068	1.129	16.774	0.0012
1264	7.626	3.294	0.070	1.133	16.803	0.0012
2528	15.252	3.289	0.069	1.134	16.906	0.0012
5056	30.504	3.330	0.065	1.135	16.899	0.0011
Average		3.311	0.069	1.131	16.880	

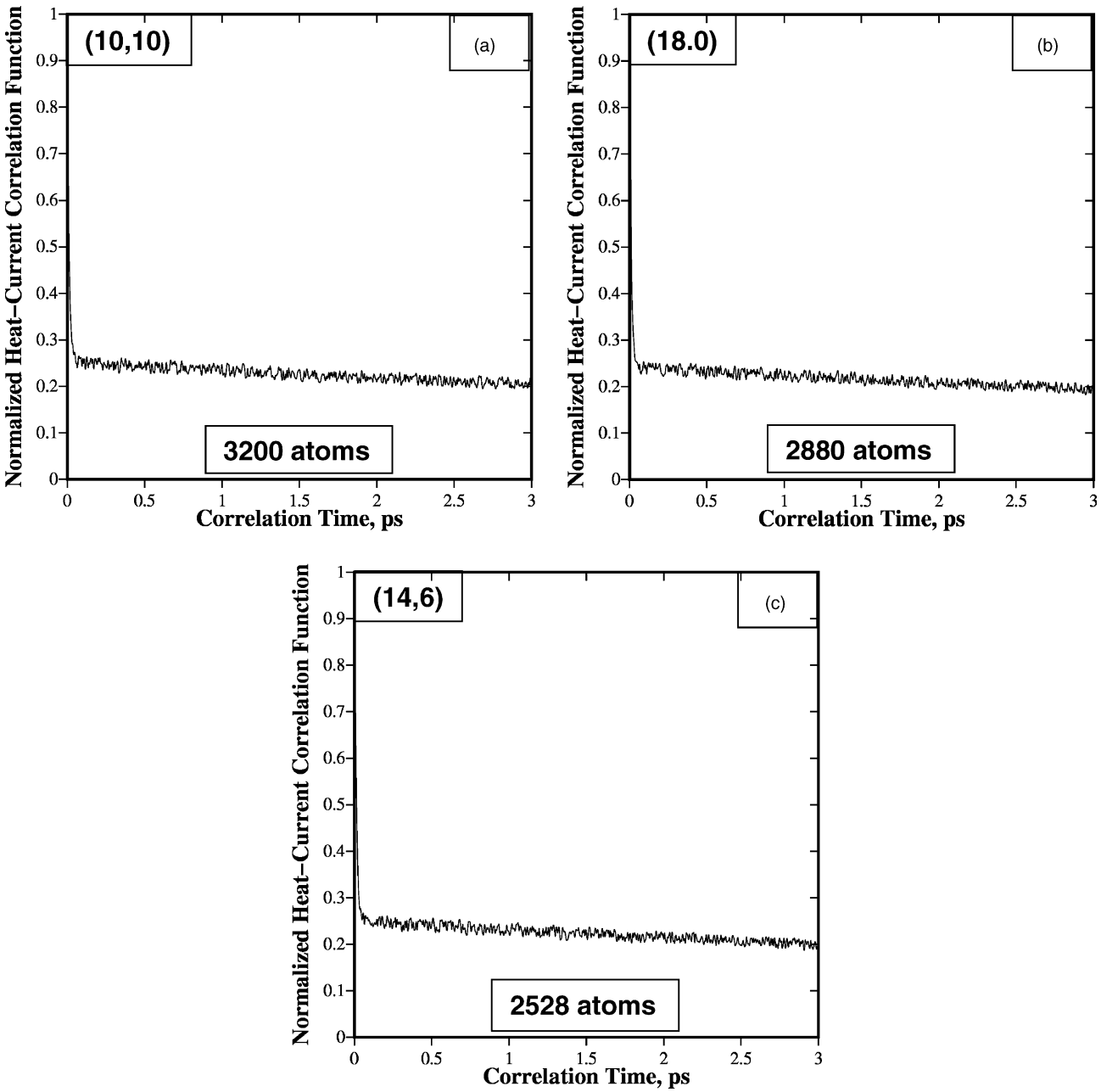

Fig. 2. Heat-current auto-correlation functions for: (a) a (10, 10); (b) a (18, 0) and (c) a (14, 6) single-walled carbon nanotube at 300 K.

of Eq. (16) in Eq. (4) yields the following expression for thermal conductivity:

$$\lambda = \frac{1}{k_B T^2 V}(A_0\tau_0 + A_a\tau_a). \quad (17)$$

Following the procedure suggested by Che et al. [2], the auto-correlation function results for all simulation runs corresponding to the first 3 ps of the correlation time are fitted to the function defined in Eq. (16) to determine the parameters A_o, τ_o, A_a, and τ_a. The results of this procedure are given in Tables 2–4. A simple analysis of the results shown in Tables 2–4 indicates that the contribution of high-frequency optical phonon modes to thermal conductivity, $(A_o\tau_o)/(A_o\tau_o + A_a\tau_a)$, is indeed very small is typically around 0.1%.

The dependence of thermal conductivity in the three types of carbon nanotubes analyzed in the present work on the size of the simulation cell is displayed in Fig. 3(a)–(c). The error bars shown in Fig. 3(a) and (b) correspond to ±1 standard deviation for the results of five molecular dynamics runs. The results displayed in Fig. 3(a)–(c) show that, as expected, when the simulation cell is too small (i.e. contains less than ~1000 atoms), the atoms in a region of the simulation cell do not have enough time to lose their previous dynamic information before a periodically equivalent phonon arrives in this region. Consequently, since the corresponding corre-

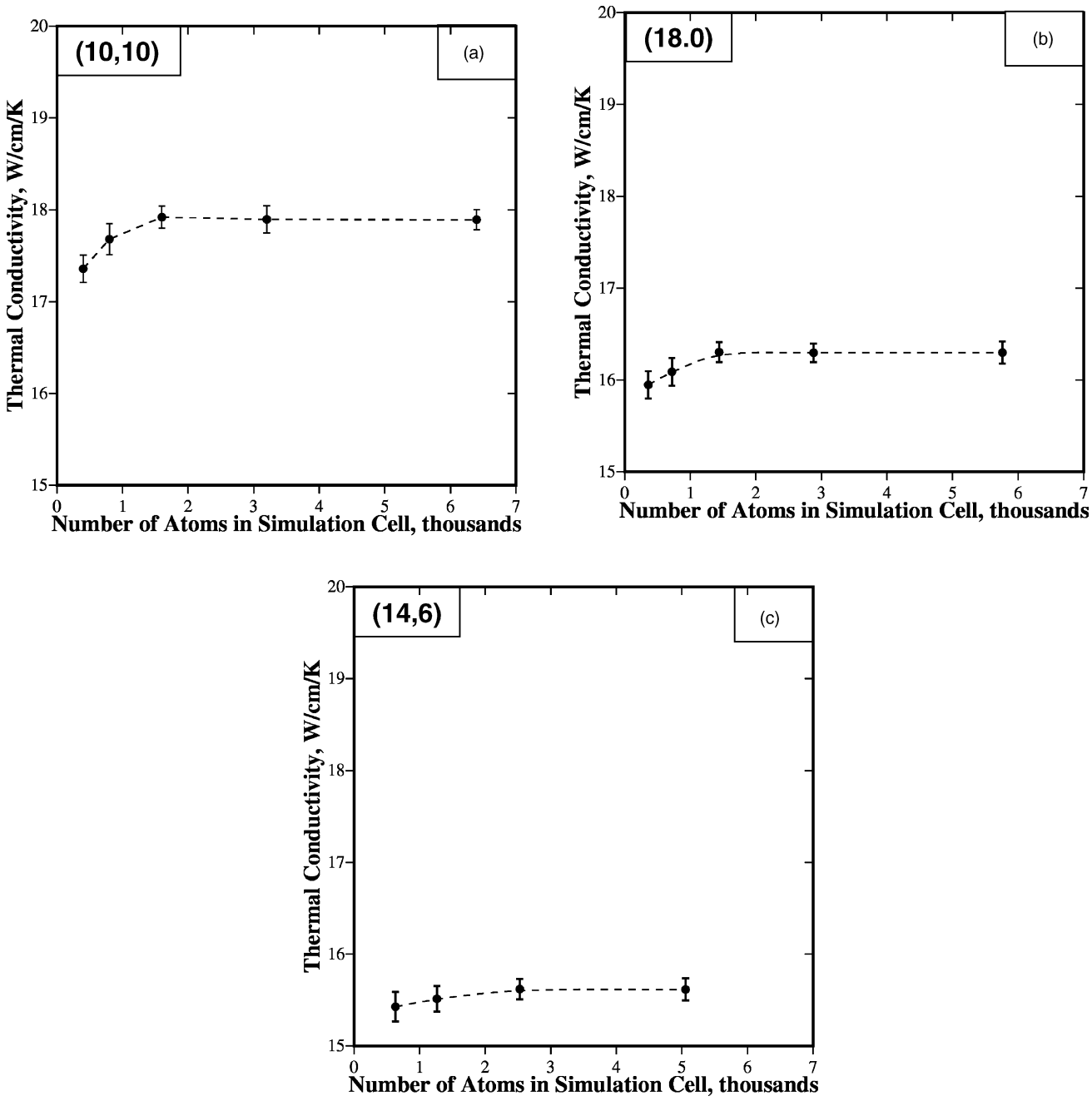

Fig. 3. Lattice thermal conductivity in: (a) a (10, 10); (b) a (18, 0) and (c) a (14, 6) single-walled carbon nanotube at 300 K.

lation functions are contaminated by such memory effects and they do not reflect behavior of the real system, computed thermal conductivity is not very accurate. On the other hand, when the computational cell size is sufficiently large, computed thermal conductivity is accurate and, essentially, independent of the size of the computational cell. The results shown in Fig. 3(a)–(c) suggest that the minimum "critical" size of the computational cell, corresponding to the maximum correlation time of 3 ps, is around 15–20 nm and is associated with cells containing approximately 3000–3500 atoms.

The analysis presented above established a minimum critical computation cell size beyond which the cell size does not affect thermal conductivity. It is interesting to determine how the critical cell size compares with the phonon mean free path in single-walled carbon nanotubes. To estimate the phonon mean free path, L, the following relation form the kinetic theory of solids is used [20]:

$$\lambda \approx \tfrac{1}{3} C_{\mathrm{v}} \rho v L \tag{18}$$

where C_{v} is the mass-based constant-volume specific heat and v is the speed of sound. The molecular dynamics

simulations carried out in the present work yielded the mean interatomic spacing of 0.142 nm. The density of single-walled carbon nanotubes is difficult to determine since they are one-atom thick. Since single-walled carbon nanotubes are typically bundled in ropes with a triangular arrangement of the nanotubes and an inter-tube spacing equal to the Van der Walls radius of carbon (0.17 nm), the nanotubes' wall thickness is set equal to this value. This procedure yielded the density of $\rho = 2.3\,\mathrm{g/cm^3}$. The experimental values for the specific heat of $C_\mathrm{v} = 500\,\mathrm{J/(kg\,K)}$ and for compressibility of $\beta_\mathrm{T} = 0.024\,\mathrm{GPa^{-1}}$ for single-walled carbon nanotubes of comparable diameters has been taken from Refs. [21,22]. Using the following equation: $v = 1/\sqrt{\rho\beta_\mathrm{T}}$, the speed of sound has been computed as 4256 m/s, Lastly, using the average thermal conductivity for the three types of nanotubes, $\lambda = 16.5\,\mathrm{W/(cm\,K)}$, and Eq. (18), the mean free path for acoustic phonons of $L = 1000$ nm has been obtained. Thus, the acoustic phonon mean free path is larger the critical computational cell size by a factor of 50–65.

The finding presented above shows that despite the fact that the phonon mean free path is considerably larger than the sizes of computational cells used, convergence in thermal conductivity can be obtained, Fig. 3(a)–(c). It should be noted that in order to set the computational cell size comparable with the phonon mean free path, computational cells containing on the order of 10^7–10^8 atoms would have to be used. Molecular dynamics simulations using such a large number of atoms, while feasible particularly if an advantage is taken of the parallel computing, would be computational very expensive and are not very appealing. Instead, as initially shown by Che et al. [2] and also confirmed in the present work, smaller size simulation cells and short-time heat-current auto-correlation functions can be used to determine thermal conductivity.

The values of the weighting factors A_o and A_a and the corresponding exponential decay constants τ_o and τ_a obtained by the nonlinear least-squares fitting of the heat-current auto-correlation functions in the three types of nanotubes and for the simulation cells with different numbers of atoms are listed in Tables 2–4. To determine the average values of these parameters, the weighting factors A_o and A_a are normalized by the nanotube volume, weighted by the number of atoms in each simulation and averaged over all simulations for a given type of nanotube. Similar averaging without volume normalization is used to obtain average values for the relaxation times, τ_o and τ_a. The results of this procedure are listed in Tables 2–4 in the row denoted as "average".

3.2. The effect of chirality

The results displayed in Fig. 3(a)–(c) further show that chirality has an effect on the lattice part of thermal conductivity in single-walled carbon nanotubes. Specifically, thermal conductivity is the highest ($\lambda = 17.8\,\mathrm{W/(cm\,K)}$) in the (10, 10) arm-chair nanotube and the lowest ($\lambda = 15.6\,\mathrm{W/(cm\,K)}$) in the (14, 6) nanotube of general chirality. Since these results pertain to the lattice contribution to thermal conductivity alone, they have to be attributed to differences in phonon-phonon interactions and the resulting differences in mean free path in the three types of nanotubes. As stated earlier, detailed modeling phonon–phonon interactions is very complicated [13] and it is beyond the scope of the present study. Nevertheless, it is well established that lattice thermal conductivity is controlled by the so-called Umklapp phonon collisions represented as: $k_1 + k_2 = k_3 + G$, where k_1 and k_2 are wave vectors of the colliding phonons, k_3 the wave vector of the resulting phonon and G is 2π times a reciprocal lattice vector. Due to differences in chirality and the resulting differences in magnitudes of the periodic length in the axial direction, one could expect differences in the permissible G vectors and, hence, lattice thermal conductivity in the three nanotubes analyzed.

It should be noted that, based on the magnitude of the band gap alone, the electronic contribution to thermal conductivity can also be expected to be the highest in the (10, 10) nanotube and the lowest in the (14, 6) nanotube. It should be noted, however, that in addition to the band gap, the electronic band structure as well as electron–electron and electron–phonon scattering also affect the electronic contribution to thermal conductivity. Nevertheless, the observation that lattice thermal conductivity can vary by as much as 20% with nanotube chirality and that electronic thermal conductivity can be affected in the same direction by chirality, suggests that thermal conductivity of individual single-walled nanotubes in nanotube ropes (consist of nanotubes of various chirality) can vary substantially from one nanotube to the other.

3.3. The effect of temperature

The molecular dynamics based procedure for computation of the thermal conductivity in single-walled carbon nanotubes described in Sections 2.1 and 2.2 is utilized in this section to determine the temperature dependence of thermal conductivity in these materials. Over the last few years, there has been a number of experimental and theoretical investigations of the effect of temperature on the thermal conductivity of single-walled carbon nanotube bundles and of individual multi-walled carbon nanotubes [31–35]. However, no reliable experimental data presently exist for the thermal conductivity of individual single-walled carbon nanotubes.

The effect of temperature in a range between 50 and 400 K on the mean value of thermal conductivity in the three types on single-walled carbon nanotubes analyzed in the present work is shown in Fig. 4. At the lowest temperature explored, thermal conductivity increases with an increase in temperature while in the upper portion of the temperature range examined, thermal conductivity decreases with an increase in temperature. This finding suggests that, at low temperatures, thermal conductivity is dominated by acoustic phonons while, at high temperatures, phonon-phonon

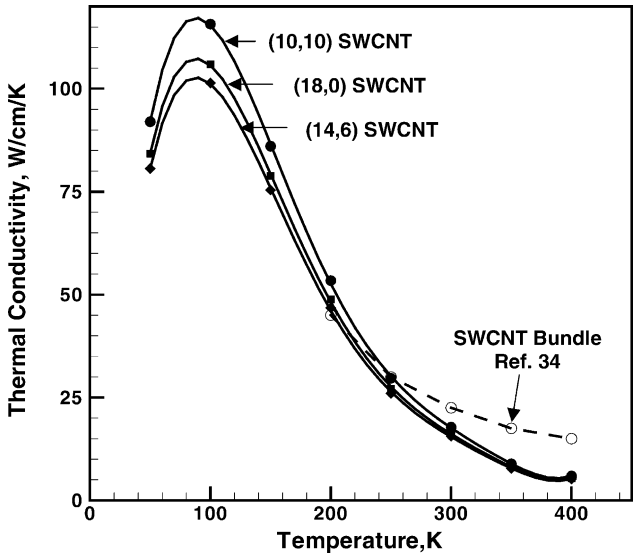

Fig. 4. The effect of temperature on the thermal conductivity in the three types of single-walled carbon nanotubes analyzed in the present work.

umklapp scattering causes the thermal conductivity to decrease with an increase in temperature [32].

For comparison, experimental results pertaining to the effect of temperature on the thermal conductivity in a bundle of the single-walled carbon nanotubes are also displayed in Fig. 4 [34]. While the agreement between the computational and the experimental results in the common temperature range can be characterized as only fair, the true validation of the present computational model entails the experimental thermal conductivities of isolated single-walled carbon nanotubes with the known chirality. Unfortunately, as stated earlier, such experimental data are presently not available.

3.4. A comparison with the Boltzmann transport equation

In this section, the equation of phonon radiative transport (EPRT) [29], derived from the Boltzmann transport equation [30] is used to compute lattice thermal conductivity of carbon nanotubes and compare it with the results presented in the previous sections. Since details of this calculation will be presented in a future communication, only a brief overview of the EPRT approach will be given here. For a one-dimensional case, the EPRT equation is defined as:

$$\frac{1}{v}\frac{\partial I_\omega}{\partial t} + \mu\frac{\partial I_\omega}{\partial x} = \frac{0.5\int_{-1}^{1} I_\omega \, \mathrm{d}\mu - I_\omega}{v\tau_\mathrm{R}} \tag{19}$$

where I_ω is the flux of energy in the direction of phonon propagation per unit area, per unit solid angle, per unit frequency, t is time, x the nanotube axial direction, ω frequency and $\mu = \cos\theta$ (θ the polar angle), τ_R the phonon relaxation time.

Eq. (19) is applied to the case of a 10 μm long nanotube, subjected at $t = 0$ to a temperature difference of 0.1 K between its ends and solved using a first-order upward finite difference method. In these calculation, $\tau_\mathrm{R} = \tau_\mathrm{a} = 17$ ps is used. The calculations of I_ω are carried out until a steady state is reached and then to integrations procedures are applied to compute the temperature and the heat flux. The resulting steady state temperature and heat flux distributions along the nanotube length are shown in Fig. 5(a) and (b), respectively. It should be noted that a normalized temperature axis, $(T(\mathrm{K}) - 300.0)/0.1$, is used in Fig. 5(a) and normalized length axes, x (μm)/0.1, are used in Fig. 5(a) and (b).

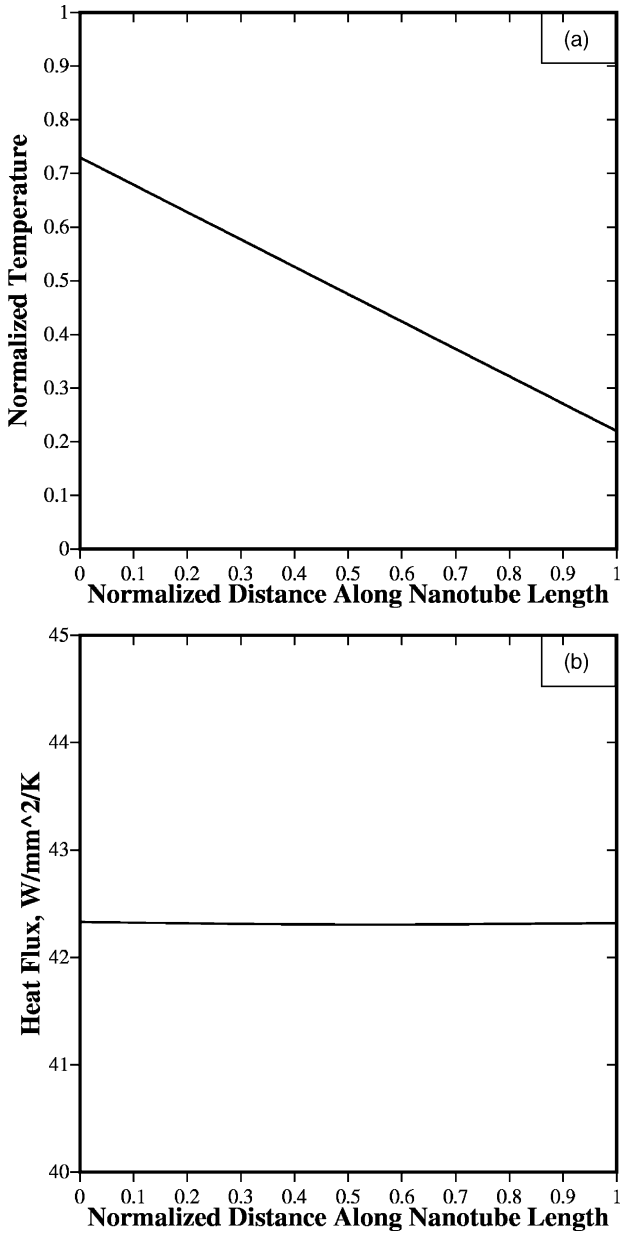

Fig. 5. Steady-state temperature (a) and heat flux (b) distributions along the nanotube length computed using the Equation of Phonon Radiative Transfer (29).

Using the results shown in Fig. 5(a) and (b) and a one-dimensional form of the steady-state Fourier heat-conduction equation, Eq. (1), thermal conductivity is

computed as 8.3 W/(cm K). This value is smaller by a factor of ∼2 than its counterparts displayed in Fig. 3(a)–(c).

4. Conclusions

Based on the results obtained in the present work, the following main conclusions can be drawn:

1. Due to an exponential-decay character of the long-time current-energy auto-correlation functions, the lattice contribution to thermal conductivity of single-walled carbon nanotubes can be determined quite accurately using molecular dynamics simulations and computational cells substantially smaller than the phonon mean free path.
2. The lattice contribution to thermal conductivity can vary by as much as 20% in single-walled carbon nanotubes depending on their chirality.
3. The lattice contributions to thermal conductivity computed using molecular dynamics based thermal-current auto-correlation functions and the ones computed using the Boltzmann transport equation agree within a factor of two with each other.

Acknowledgements

The material presented in this paper is based on work supported by the US Army Grant Number DAAD19-01-1-0661. The authors are indebted to Drs. Walter Roy, Fred Stenton and William DeRosset of ARL for the support and a continuing interest in the present work. The authors also acknowledge the help of Professor R.S. Miller with the EPRT calculations.

Appendix A. The adaptive intermolecular reactive empirical bond order (AIREBO) potential

The Brenner's Reactive Empirical Bond Order (REBO) potential [18,24–26] is an interactive potential initially developed to model the covalent bonding interactions in carbon and hydrocarbon systems attending Chemical Vapor Depositions (CVD) of diamond. While this potential and its various incarnations have been recently extended to analyze energetic, elastic and vibrational properties of fullerenes [26], carbon nanotubes [27], amorphous carbon [28], etc. they are not the most appropriate for such analyses due to significant contribution of nonbonding (intermolecular) interactions which the REBO potential does not include. Recently, Stuart et al. [17] upgraded the REBO potential by including an adaptive treatment of the interactions involving nonbonded atoms and dihedral–angle intermolecular interactions. This potential, named the Adaptive Intermolecular Reactive Empirical Bond Order (AIREBO) potential is briefly overviewed in this section.

Within the AIREBO potential formulation, the potential energy of a system of atoms is represented as [17]:

$$E = \frac{1}{2}\sum_i \sum_{j\neq i} \left[E_{ij}^{\mathrm{REBO}} + E_{ij}^{\mathrm{LJ}} + \sum_{k\neq i,j} \sum_{l\neq i,j,k} E_{kijl}^{\mathrm{tors}} \right] \quad (A.1)$$

The REBO potential, E_{ij}^{REBO}, describes the interactions between covalently-bonded atoms (the intramolecular interactions), while the dispersion and intermolecular repulsion interactions between nonbonded atoms are accounted for through the use of the Lennard-Jones (LJ) E_{ij}^{LJ} term. The last term in Eq. (A.1) is used to describe dihedral–angle intermolecular interactions which are deemed not significant in the analysis of carbon nanotubes [17] and, hence, this term is not considered in the present work.

The REBO interaction term, E_{ij}^{REBO}, is defined as [18]:

$$E_{ij}^{\mathrm{REBO}} = V_{ij}^{\mathrm{R}} + b_{ij} V_{ij}^{\mathrm{A}} \quad (A.2)$$

where the repulsive, V_{ij}^{R}, and the attractive, V_{ij}^{A}, interaction energies between atoms i and j separated by r_{ij} in Eq. (A.2) are combined in a ratio determined by the many-body bonding parameter, b_{ij}. The repulsive term is defined as [18]:

$$V_{ij}^{\mathrm{R}} = w_{IJ}(r_{ij}) \left[1 + \frac{Q_{ij}}{r_{ij}} \right] A_{ij}\, \mathrm{e}^{-\alpha_{ij} r_{ij}} \quad (A.3)$$

where the parameters Q_{ij}, A_{ij}, and α_{ij} depend on the atom types i and j. Values for these and all other REBO potential parameters can be found in Table 2, Ref. [17]. The w_{IJ} term in Eq. (A.3) is a bond–weighting function defined as:

$$w_{ij}(r_{ij}) = S'(t_{\mathrm{c}}(r_{ij})), \quad (A.4)$$

which is used to switch off the REBO interactions, in a continuous manner, when the distance between atoms i and j exceeds an atomic-type dependent bonding distance and the i–j bond breaks. The switching function, $S'(t_{\mathrm{c}}(r_{ij}))$, and the scaling function, $t_{\mathrm{c}}(r_{ij})$, are defined as:

$$S'(t) = \Theta(-t) + \Theta(t)\Theta(1-t)\tfrac{1}{2}[1 + \cos(\pi t)] \quad (A.5)$$

and

$$t_{\mathrm{c}}(r_{ij}) = \frac{r_{ij} - r_{ij}^{\min}}{r_{ij}^{\max} - r_{ij}^{\min}} \quad (A.6)$$

respectively, while the switching region is defined in terms of $r_{ij}^{\min}$ and $r_{ij}^{\max}$. Θ in Eq. (A.5) denotes the Heaviside step functions, $S'(t)$ is unity for $t < 0$ and zero for $t > 1$ and provides a smooth switching between these two values for $0 < t < 1$.

The attractive pair interaction term in Eq. (A.2) is given by a triple exponential function as [18]:

$$V_{ij}^{\mathrm{A}} = -w_{IJ}(r_{ij}) \sum_{n=1}^{3} B_{ij}^{(n)}\, \mathrm{e}^{-\beta_{ij}^{(n)} r_{ij}} \quad (A.7)$$

and is switched off smoothly over the same switching region as V_{ij}^{R} through the use of the bond weighting function $w_{IJ}(r_{ij})$.

The many-body bonding term, b_{ij}, in Eq. (A.2) defines the "bond order" for the interaction between atoms i and j (the larger b_{ij}, the stronger the i–j bond), by making the strength of the i–j bond dependent on the local atomic environment and is given as:

$$b_{ij} = \tfrac{1}{2}[p_{ij}^{\sigma\pi} + p_{ji}^{\sigma\pi}] + \pi_{ij}^{\mathrm{rc}} + \pi_{ij}^{\mathrm{dh}} \tag{A.8}$$

The principal contribution to b_{ij} in Eq. (A.8) comes from the covalent-bond interaction terms, $p_{ij}^{\sigma\pi}$, and $p_{ji}^{\sigma\pi}$ ($p_{ij}^{\sigma\pi}$ is not necessarily equal to $p_{ji}^{\sigma\pi}$), where $p_{ij}^{\sigma\pi}$ is defined as:

$$p_{ij}^{\sigma\pi} = \left[1 + \sum_{k\neq i,j} w_{ij}(r_{ik}) g_i(\cos\theta_{jik})\, \mathrm{e}^{\lambda_{jik}} + P_{ij}\right]^{-1/2} \tag{A.9}$$

where θ_{jik} is the bond angle between the r_{ji} vector connecting neighboring atoms j and i and the vectors r_{ki} connecting atom i to another neighboring atom k. The penalty function, g_i, in Eq. (A.9), is used to provide an increase in the energy for bonds that are too close to one another and its functional form is a fifth-order spline. The coefficients of the spline are listed in Table 7, Ref. [17].

The two remaining terms in Eq. (A.9) represent relatively small correction factors. The $\mathrm{e}^{\lambda_{jik}}$ term is added to improve the potential energy surface for abstraction of hydrogen atoms from hydrocarbons while the P_{ij} term (a two dimensional cubic spline) is used to obtain accurate bond energies for small hydrocarbons. The parameters for these two terms are given, respectively, in Tables 2 and 8, Ref. [17].

In addition to the covalent-bonding interactions given by Eq. (A.9), the REBO potential also includes contributions to the bond order from radical and conjugation effects. These enter the potential through the π_{ij}^{rc} term in Eq. (A.8), which is a three dimensional cubic spline of N_{ij}, N_{ji}, and N_{ij}^{conj} as independent variables. N_{ij} and N_{ji} are, respectively, atoms i and j coordination numbers, while N_{ij}^{conj} is a local measure of conjugation in the i–j bond and is given as:

$$N_{ij}^{\mathrm{Conj}} = 1 + \left[\sum_{k\neq i,j} \delta_{kC} w_{ik}(r_{ik}) S'(t_{\mathrm{conj}}(N_{ki}))\right]^2 + \left[\sum_{l\neq i,j} \delta_{lC} w_{jl}(r_{jl}) S'(t_{\mathrm{conj}}(N_{lj}))\right]^2 \tag{A.10}$$

t_{conj} in Eq. (A.10) specifies the range of coordination numbers under which a bond is assumed to be part of a radical or conjugated network and is defined as:

$$t_{\mathrm{conj}}(N_{ij}^{\mathrm{conj}}) = \frac{N_{ij}^{\mathrm{conj}} - N_{ij}^{\mathrm{conj,min}}}{N_{ij}^{\mathrm{conj,max}} - N_{ij}^{\mathrm{conj,min}}} \tag{A.11}$$

The N_{ij}^{conj} variable, which is unity for nonconjugated bonds and can be as high as nine in polyaromatic compounds, is an empirical measure of unsaturation that is dependent entirely on local coordination. The interpolation points for the three-dimensional spline, π_{ij}^{rc}, are provided in Table 9, Ref. [17].

The last contribution to the bond order b_{ij} in Eq. (A.8) is π_{ij}^{dh}. This term imposes a penalty for rotation around multiple bonds and is defined as:

$$\pi_{ij}^{\mathrm{dh}} = T_{ij}(N_{ij}, N_{ji}, N_{ij}^{\mathrm{conj}}) \sum_{k\neq i,j} \sum_{l\neq i,j} (1 - \cos^2\omega_{kijl}) \times w'_{ik}(r_{ik}) w'_{jl}(r_{jl}) \Theta(\sin(\theta_{jik}) - s^{\min}) \times \Theta(\sin(\theta_{ijl}) - s^{\min}) \tag{A.12}$$

where T_{ij} is a three-dimensional cubic spline, with interpolation points given in Table 10, Ref. [17]. The torsion angle ω_{kijl} is defined as the angle between the plane defined by the vectors r_{ik} and r_{ij} and that defined by the vectors r_{ij} and r_{jl} as:

$$\cos\omega_{kijl} = \frac{r_{ji} \times r_{ik}}{|r_{ji} \times r_{ik}|} \cdot \frac{r_{ij} \times r_{jl}}{|r_{ij} \times r_{jl}|} \tag{A.13}$$

The bond weighting function, $w'(r_{ij})$, used in Eq. (A.12) is defined as:

$$w'_{ij}(r_{ij}) = S'(t'_{\mathrm{c}}(r_{ij})) \tag{A.14}$$

and differs slightly from that defined in Eq. (A.4), through a different scaling function t'_{c} defined as:

$$t'_{\mathrm{c}}(r_{ij}) = \frac{r_{ij} - r_{ij}^{\min}}{r_{ij}^{\max} - r_{ij}^{\min}} \tag{A.15}$$

The E_{ij}^{LJ} term in Eq. (A.1) is based on the Lennard-Jones (LJ) 12–6 potential and is defined as:

$$V_{ij}^{\mathrm{LJ}}(r_{ij}) = 4\varepsilon_{ij}\left[\left(\frac{\sigma_{ij}}{r_{ij}}\right)^{12} - \left(\frac{\sigma_{ij}}{r_{ij}}\right)^{6}\right] \tag{A.16}$$

The inclusion of the LJ term creates several challenges, foremost of these is introduction of a steep repulsive wall, which prevents unbonded atoms (atoms associated with different molecules) from getting close enough to interact via the REBO potential. Rather than overcoming this problem by incorprating a simple distance-dependent switching function in the LJ potential, and thus neglecting the effect of chemical environment, Stuart et al. [17] introduced three criteria to switch on or off the LJ interactions in an adaptive fashion. The three criteria are based on: (a) the separation distance between the two atoms in question; (b) their bond order; and (c) the network of covalent bonds connecting the atoms. Consequently the LJ interaction term in Eq. (A.1) is defined as:

$$E_{ij}^{\mathrm{LJ}} = S(t_{\mathrm{r}}(r_{ij}))S(t_{\mathrm{b}}(b_{ij}^{*})C_{ij}V_{ij}^{\mathrm{LJ}}(r_{ij}) + [1 - S(t_{\mathrm{r}}(r_{ij}))]C_{ij}V_{ij}^{\mathrm{LJ}}(r_{ij}), \tag{A.17}$$

where the atomic-separation-distance based switching function, $S(t)$, is given as:

$$S(t) = \Theta(-t) + \Theta(t)\Theta(1-t)[1 - t^2(3 - 2t)] \tag{A.18}$$

and the scaling function, $t_r(r_{ij})$, in Eq. (A.17) is given as:

$$t_r(r_{ij}) = \frac{r_{ij} - r_{ij}^{\mathrm{LJ\,min}}}{r_{ij}^{\mathrm{LJ\,max}} - r_{ij}^{\mathrm{LJ\,min}}} \tag{A.19}$$

When $r_{ij} > r_{ij}^{\mathrm{LJ\,max}}$, $S(t_r(r_{ij})) = 0$ and the magnitude of the i–j atomic separation distance, r_{ij}, has no effect on the LJ interactions. When $r_{ij} < r_{ij}^{\mathrm{LJ\,max}}$, on the other hand, the first-term in Eq. (A.17) is non zero and the LJ interactions are contingent on the values of $S(t_b(b_{ij}^*))$ and C_{ij}.

The switching region $[r_{ij}^{\mathrm{LJ\,min}}, r_{ij}^{\mathrm{LJ\,max}}]$ in Eq. (A.19) is chosen such that no artificial reaction barrier is introduced due to LJ repulsions at short distances ($r_{ij}^{\mathrm{LJ\,min}} = \sigma_{ij}$) and that switching off leaves the minimum of the LJ potential function unperturbed ($r_{ij}^{\mathrm{LJ\,max}} = 2^{1/6}\sigma_{ij}$).

The second (bond strength) criterion affecting the LJ interactions is included through the use of the $S(t_b(b_{ij}^*))$ switching function in Eq. (A.17) where the scaling function $t_b(b_{ij})$ is given as:

$$t_b(b_{ij}) = \frac{b_{ij}^* - b_{ij}^{\mathrm{LJ\,min}}}{b_{ij}^{\mathrm{max}} - b_{ij}^{\mathrm{min}}} \tag{A.20}$$

When the two atoms in question are covalently bonded, (the bond-order parameter, b_{ij}^*, is large and, hence, $t_b \geq 1$ and $S(t_b(b_{ij}^*)) = 0$), the repulsive LJ interactions (represented by the first term in Eq. (A.17)) vanishes. For lower values of the bond order parameter, on the other hand, the LJ interactions will be included to a variable degree depending on the value of b_{ij}^*. For sufficiently small values of b_{ij}^* (which indicates that covalent bonding is not likely), $S(t_b(b_{ij}^*)) = 1$, and the LJ repulsion interactions are undiminished.

It should be noted that separations between nonbonded atoms generally exceed the maximum covalent bonding distance, r_{ij}^{max} in Eq. (A.6), and hence the REBO parameter, b_{ij}, does not provide an accurate representations of the bond order. To overcome this problem, the AIREBO bond order parameter for non-bonded i–j atomic interactions, b_{ij}^*, is represented by a hypothetical REBO b_{ij} term evaluated at r_{ij}^{min} with the distances between atoms i and j to each of their neighbors being kept unchanged.

The third criterion governing the LJ interactions is represented by the connectivity switch C_{ij} in Eq. (A.17) and is introduced to suppress LJ interactions between first neighbors (1–2), second neighbors (1–3) and third neighbors (1–4) which are either well described by the REBO potential or by the dihedral-angle potential described below. To derive an expression for C_{ij}, a bond weight function $w_{ij}(r)_{ij}$ is first defined to enable a smooth transition between bonded ($w_{ij} = 1$) and nonbonded ($w_{ij} = 0$) atomic interactions. The bond weight function is given as:

$$w_{ij}(r_{ij}) = S'(t_c(r_{ij})) \tag{A.21}$$

where the switching function $S'(t)$ is given as:

$$S'(t) = \Theta(-t) + \Theta(t)\Theta(1-t)\tfrac{1}{2}[1 + \cos(\pi t)] \tag{A.22}$$

while the scaling function $t_c(r_{ij})$ is defined as:

$$t_c(r_{ij}) = \frac{r_{ij} - r_{ij}^{\mathrm{min}}}{r_{ij}^{\mathrm{max}} - r_{ij}^{\mathrm{min}}} \tag{A.23}$$

To exclude (1–2), (1–3) and (1–4) LJ interactions, the connectivity switch C_{ij} is defined as:

$$C_{ij} = 1 - \max\{w_{ij}(r_{ij}), w_{ik}(r_{ik})w_{kj}(r_{kj}), \quad \forall k; \\ w_{ik}(r_{ik})w_{kl}(r_{kl})w_{lj}(r_{lj}), \quad \forall k, l\} \tag{A.24}$$

Thus, when atoms i and j are neighbors ($w_{ij}(r_{ij}) = 1$) or connected by one ($w_{ik}(r_{ik})w_{kj}(r_{kj}) = 1$) or two ($w_{ik}(r_{ik}) \cdot w_{kl}(r_{kl}) \cdot w_{lj}(r_{lj}) = 1$) neighbors, $C_{ij} = 0$ and there are no LJ interactions between the atoms.

In summary, the strength of LJ interactions is affected by atomic separation distance, bond order and connectivity. For the LJ interactions to be fully included, the atom pairs in question must not be first, second or third neighbors and must either be beyond a cut-off distance or have a very low value of the bond order.

References

[1] P. Stachowiak, V.V. Sumarokov, J. Mucha, A. Jezowski, Phys. Rev. B 58 (1998) 2380.
[2] J. Che, T. Cagin, W. Deng, W.A. Goddard III, J. Chem. Phys. 113 (2000) 6888.
[3] L. Chico, V.H. Crespi, L.X. Benedict, Phys. Rev. Lett. 76 (1996) 971.
[4] L. Langer, V. Bayot, E. Grivei, Phys. Rev. Lett. 76 (1996) 479.
[5] T.W. Ebbesen, H.J. Lezec, H. Hiura, J.W. Bennett, H.F. Ghaemi, T. Thio, Nature 382 (1996) 54.
[6] T. Pichler, M. Knupfer, M.S. Golden, Phys. Rev. Lett. 80 (1998) 4729.
[7] D.J. Evans, Phys. Lett. 91A (1982) 457.
[8] D. Macgowan, D.J. Evans, Phys Lett. A 117 (1986) 414.
[9] P.J. Davis, D.J. Evans, J. Chem. Phys. 103 (1995) 4261.
[10] S. Walkauskas, D. Broido, K. Kempa, T. Reinecke, J. Appl. Phys. 85 (1999) 2579.
[11] A. Balandin, K. Wang, Phys. Rev. B 58 (1998) 1544.
[12] V.L. Gurevich, Transport in Phonon Systems, North-Holland, Amsterdam, 1986.
[13] M.J. Gillan, Phys. Scr., T T39 (1991) 362.
[14] G.D. Mahan, Many-Particle Physics, Plenum Press, New York, 1993.
[15] R. Kubo, M. Toda, N. Hashitsume, Statistical Physics, vol. II, Springer, Berlin, 1985.
[16] G.D. Mahan, Many-Particle Physics, Plenum, New York, 1993.
[17] S.J. Stuart, A.B. Tutein, J.A. Harrison, J. Chem. Phys. 112 (2000) 6472.
[18] D.W. Brenner, S.B. Sinnott, J.A. Harrison, unpublished.
[19] H.J.C. Berendsen, J.P.M. Postma, W.F. Van Gunsteren, A. Di Nola, J.R. Haak, J. Chem. Phys. 81 (1984) 3684.
[20] J.M. Ziman, Principles of the Theory of Solids, Cambridge University Press, Cambridge, 1972.
[21] W. Yi, L. Lu, D.-L. Zhang, Z.W. Pan, S.S. Xie, Phys. Rev. B 59 (1999) R9015.
[22] J. Tang, L.-C. Qin, T. Sasaki, M. Yudasaka, A. Matsushita, S. Iijima, Phys. Rev. Lett. 85 (2000) 1887.
[23] W.H. Press, B.P. Flannery, S.A. Teukolsky, W.P. Vetterling, Numerical Recipes: The Art of Scientific Computing, Cambridge University Press, 1986.

[24] D.W. Brenner, Phys. Rev. B 42 (1990) 9458.
[25] D.W. Brenner, Phys. Rev. B 46 (1992) 1948.
[26] D.W. Brenner, J.A. Harrison, C.T. White, R.J. Colton, Thin Solid Films 206 (1991) 220.
[27] S.B. Sinnott, R.J. Colton, C.T. White, O.A. Shendeova, D.W. Brenner, J.A. Harrison, J. Vac. Sci. Technol. A 15 (1997) 936.
[28] J.A. Harrison, C.T. White, R.J. Colton, D.W. Brenner, Phys. Rev. B 46 (1992) 9700.
[29] A. Majumdar, J. Heat Transfer 115 (1993) 7.
[30] J.M. Ziman, Electrons and Phonons, Oxford University Press, London, 1960.
[31] W. Yi, L. Lu, D.L. Zhang, Z.W. Pan, S.S. Xie, Phys. Rev. B 59 (1999) R9015.
[32] J. Hone, M. Whitney, C. Piskoti, A. Zettl, Phys. Rev. B 59 (1999) R2541.
[33] P. Kim, L. Shi, A. Majumdar, P.L. McEuen, Phys. Rev. Lett. 87 (2001) 215502.
[34] S. Berber, Y.K. Kwon, D. Tomanek, Phys. Rev. Lett. 84 (2000) 4613.
[35] B.A. Glavin, Phys. Rev. Lett. 86 (2001) 4318.